Carbohydrate Polymers 352 (2025) 123140

Contents lists available at ScienceDirect

Carbohydrate Polymers

journal homepage: www.elsevier.com/locate/carbpol

Synthesis and characterization of photo-cross-linkable quince seed-based hydrogels for soft tissue engineering applications

Arman Jafari [a,b,c], Khushbu Bhatt [d], Seyyed Vahid Niknezhad [e], Abdellah Ajji [f], May Griffith [a,g,k], Gregor Andelfinger [b], Sidi A. Bencherif [h,i,j,*], Houman Savoji [a,b,c,**]

[a] Institute of Biomedical Engineering, Department of Pharmacology and Physiology, Faculty of Medicine, University of Montreal, Montreal, QC H3T 1J4, Canada
[b] Azrieli Research Center, Centre Hospitalier Universitaire Sainte-Justine, Montreal, QC H3T 1C5, Canada
[c] Montreal TransMedTech Institute, Montreal, QC H3T 1J4, Canada
[d] Department of Pharmaceutical Sciences, Northeastern University, Boston, MA 02115, United States
[e] Department of Cell and Tissue Biology, University of California, 513 Parnassus Avenue, San Francisco, CA 94143, United States
[f] CREPEC, Département de Génie Chimique, Polytechnique Montréal, Montréal, QC H3C3A7, Canada
[g] Maisonneuve-Rosemont Hospital Research Centre, Montreal, QC H1T 2H2, Canada
[h] Department of Chemical Engineering, Northeastern University, Boston, MA 02115, United States
[i] University of Rouen Normandie, CNRS, PBS UMR 6270, F-76000 Rouen, France
[j] John A. Paulson School of Engineering and Applied Sciences, Harvard University, Cambridge, MA 02128, United States
[k] Department of Ophthalmology, Faculty of Medicine, University of Montreal, QC H3T 1J4, Canada

ARTICLE INFO

Keywords:
Polysaccharide
Photosensitive
Hydrogel
Scaffold
3D printing
Tissue engineering

ABSTRACT

The convenience, versatility, and biocompatibility of photocrosslinkable hydrogel precursors make them promising candidates for developing tissue engineering scaffolds. However, the current library of photosensitive materials is limited. This study reports, for the first time, the modification of quince seed mucilage (QS) with glycidyl methacrylate (GM), resulting in the synthesis of methacrylated QS (QSGM). The chemical composition and structure of QS were analyzed. The effects of reaction time, temperature, QS concentration, and GM/QS ratio on the degree of methacrylation, as well as the physicochemical, rheological, mechanical, and biological properties of the synthesized materials were explored. Chemical characterization using ^{1}H NMR and FTIR confirmed the successful methacrylation of QS. Hydrogels fabricated from QSGMs at a 0.5 wt% concentration exhibited high swelling ratios of 320 to 580 g/g, and compressive strengths between 0.6 ± 0.1 and 1.2 ± 0.3 kPa. No significant changes in the rheological properties of hydrogel precursors were observed. Moreover, QSGM-based hydrogels supported cell encapsulation for 14 days with minimal cytotoxicity and immune cell activation. Finally, as a proof of concept, the potential use of QSGM for 3D printing was demonstrated. Overall, the results highlight the significant potential of QSGMs as a biomaterial of choice for soft tissue engineering applications.

1. Introduction

Most tissue-engineering platforms rely on developing a temporary substrate, known as a scaffold, to accelerate and enhance tissue repair and regeneration. These scaffolds can either be combined with cells or used independently to attract endogenous cells. Hydrogels are particularly valuable for constructing such scaffolds. As three-dimensional (3D) polymeric networks, hydrogels can absorb large volumes of water, allowing them to mimic the native extracellular matrix (ECM) (Jafari et al., 2024; Unagolla & Jayasuriya, 2020). Furthermore, the biocompatibility, biodegradability, and tunable physicochemical properties of hydrogels make them well-suited for developing solutions tailored to individual patients and specific tissues (Faramarzi et al., 2018; Guo et al., 2020; Kim et al., 2014).

Among the various synthetic and natural polymers used to fabricate hydrogels, polysaccharides are considered one of the most intriguing materials. They can be derived from numerous natural sources, including animals, seaweeds, insects, bacteria, and plants (Jafari et al.,

* Correspondence to: S.A. Bencherif, Department of Chemical Engineering, Northeastern University, Boston, MA 02115, United States.
** Correspondence to: H. Savoji, Institute of Biomedical Engineering, Department of Pharmacology and Physiology, Faculty of Medicine, University of Montreal, Montreal, QC H3T 1J4, Canada.
E-mail addresses: s.bencherif@northeastern.edu (S.A. Bencherif), houman.savoji@umontreal.ca (H. Savoji).

https://doi.org/10.1016/j.carbpol.2024.123140
Received 26 March 2024; Received in revised form 9 December 2024; Accepted 11 December 2024
Available online 12 December 2024

2022; Mahdavi et al., 2021; Yoon et al., 2011). These carbohydrate polymers possess key properties, including biocompatibility, biodegradability, hydrophilicity, and ease of crosslinking, making them ideal for tissue engineering applications (Jin et al., 2021; Tiwari et al., 2018). For instance, hyaluronic acid, a linear anionic glycosaminoglycan abundant in native ECM—particularly in cartilage—has been extensively used in tissue engineering (Bhatt et al., 2022; Colombani, Eggermont, Hatfield, et al., 2021; Ding et al., 2022; Tsanaktsidou et al., 2022).

Quince seed mucilage (QS) consists of water-soluble, biocompatible, and bioactive polysaccharides. Traditionally, quince seeds have been used to treat ailments such as sore throats, coughs, and bronchitis (Yilmaz et al., 2021). Several recent studies have utilized QS to develop tissue-engineered scaffolds and drug delivery systems (Darvishi et al., 2021; Ghumman et al., 2022). For instance, combining QS with cellulose nanofibrils has been proposed to create new inks that are non-cytotoxic and suitable for 3D printing into soft tissue-engineered scaffolds (Baniasadi et al., 2021).

Another notable feature of hydrogels is the versatility of crosslinking methods available for their fabrication. This flexibility allows scientists to adjust their properties for specific applications. Additionally, mild and biologically safe approaches can be employed, enabling cell incorporation into hydrogel precursors to create cell-encapsulated scaffolds or to form scaffolds in situ (Ahmad et al., 2022; Echalier et al., 2019). Free radical polymerization is the most commonly used approach for forming chemically crosslinked hydrogels (Nicodemus & Bryant, 2008). Notably, the formulation of photosensitive materials and hydrogel precursors that can be crosslinked with light-sensitive photoinitiators is of particular interest (Chen et al., 2022). Photo-crosslinking offers a straightforward approach for forming hydrogels with precise control over their spatial and temporal characteristics. Furthermore, these materials can be readily integrated with rapidly advancing (bio)fabrication techniques to develop 3D structures and scaffolds with high complexity and resolution (Echalier et al., 2019; Lim et al., 2020). Photosensitive materials can be created by functionalizing polymers with acrylate or methacrylate residues. Functional pendant groups on the backbone of a polysaccharide can react with methacrylic anhydride or glycidyl methacrylate (GM) to introduce reactive vinyl bonds into the polymer chain, enabling radical polymerization upon exposure to ultraviolet (UV) or visible light (Pereira & Bártolo, 2015). However, only a limited number of photosensitive biopolymers are currently available for use in the biomedical field to create tissue engineering scaffolds. Consequently, there is a need to develop novel photosensitive biopolymers suitable for advanced manufacturing techniques and the fabrication of engineered scaffolds for both soft and hard tissue engineering applications.

In this study, we investigated the potential of modifying QS with GM to produce glycidyl methacrylate-grafted QS (QSGM), capable of forming hydrogels upon light exposure. To the best of our knowledge, no previous work has reported the development of QSGM. Several reaction conditions were tested to investigate the effects of reaction time, temperature, QS concentration, and GM/QS ratio on the degree of methacrylation. Hydrogel precursors were prepared from the synthesized QSGMs, and their rheological, physical, and mechanical properties were recorded. Cell cytotoxicity and viability of 3 T3 fibroblasts embedded in the hydrogels were also investigated. Additionally, the immune cell activation response induced by QS and the hydrogels was examined. Finally, QSGMs were used to 3D print scaffolds with various geometries to assess their compatibility with advanced biofabrication approaches.

2. Materials and methods

2.1. Materials

Quince seeds were purchased from a local store (Tavazo Nuts & Fruits, Toronto, Canada). Glycidyl methacrylate (GM), sodium formate (SF), Lithium phenyl-2,4,6-trimethylbenzoylphosphinate (LAP), 4-Methoxyphenol (MEHQ), Sodium hydroxide (NaOH), and NH_4OH were obtained from Sigma-Aldrich. Carbopol ETD 2020 was provided as a kind gift from Lubrizol, USA. Deuterium oxide (D_2O, 99.9 %) was supplied by ACP Chemicals, Canada. LIVE/DEAD™ Viability/Cytotoxicity Kit was purchased from Invitrogen. Purified Milli-Q (deionized, demineralized) water was utilized throughout the experiments.

2.2. Extraction of QS

To extract QS, 20 g of dry quince seeds were soaked in one liter of Milli-Q water and stirred at 40 °C for 24 h. The resulting QS-rich suspension was centrifuged at 4000 rpm for 10 min to separate the seeds from the solution. The supernatant was then poured into ethanol to precipitate the QS, which was subsequently redissolved in Milli-Q water and freeze-dried. Finally, the lyophilized QS was stored at −20 °C until further use.

2.3. Composition analysis by trimethylsilyl (TMS) derivatization and gas chromatography–mass spectrometry (GC–MS)

The glycosyl composition of QS was analyzed by forming per-*O*-trimethylsilyl (TMS) methyl glycosides, following the method described previously (Coleman et al., 2019). Dried samples were treated with 1 M methanolic HCl at 80 °C to depolymerize the polysaccharide and convert the resulting monosaccharides into methyl glycosides. Reacetylation was performed by adding methanol, pyridine, and acetic anhydride to the dry sample for 15 min at room temperature. The sample was then derivatized with TMS reagent (Tri-Sil HTP reagent, Thermo, USA) at 80 °C for 20 min. The resulting TMS methyl glycosides were dissolved in 200 μL of hexane and transferred to a GC vial. GC–MS analysis was conducted on an Agilent 7890 A GC interfaced with a 5975C MSD, using a Supelco Equity-1 fused silica capillary column (30 m × 0.25 mm ID). The initial temperature of 80 °C was held for 2 min, then ramped at 2 °C/min to 200 °C, followed by a 2-min hold, and finally increased at 30 °C/min to 250 °C, where it was maintained for 5 min.

2.4. Linkage analysis by partially methylated alditol acetate (PMAAs) and GC–MS

Methylation of QS was carried out by dissolving QS in DMSO, followed by the addition of NaOH and iodomethane. Subsequently, 2 M trifluoroacetic acid was added to the sample, which was then heated at 120 °C for 2 h. To reduce the anomeric group, $NaBH_4$ (10 mg/mL in NH_4OH) was added to the sample and allowed to react overnight. Acetylation was performed by adding acetic anhydride and TFA to the QS and reacting it at 35 °C for 20 min. The sample was then extracted with 2 mL of DCM, and the DCM layer was washed five times with 2 mL of water. The resulting partially methylated alditol acetates (PMAAs) were analyzed using an Agilent 7890 A GC interfaced with a 5975C MSD, with separation on a Supelco 2331 fused silica capillary column (30 m × 0.25 mm ID). The temperature gradient was set as follows: an initial temperature of 60 °C held for 1 min, followed by an increase of 4 °C/min to 235 °C with a 2-min hold, and then an increase of 3 °C/min to 240 °C, where it was held for 12 min.

2.5. Synthesis of photosensitive QS

QS was modified using GM as the photosensitive modifier. QS at different concentrations (0.25 and 0.5 wt./v%) was dissolved in Milli-Q water, and MEHQ was added at 0.5 wt% to all reactants. MEHQ acts as an inhibitor, preventing radical polymerization and the activation of GM's unsaturated double bonds during the reaction (Davenport Huyer et al., 2019). The pH of the solution was adjusted to approximately 3.5 using 1 M HCl. Once the predefined temperature (Table 1) was reached, GM was added dropwise to the solution, and the container was shielded from light exposure. After the reaction was complete, the solution was

Table 1
Reaction conditions used to synthesize photopolymerizable QSGM and their sample code designation.

Sample code	QS concentration (wt./v%)	GM/QS ratio (w/v)	Reaction temperature (°C)	Reaction time (h)
QSGM1	0.5	5	60	24
QSGM2	0.5	5	RT[a]	24
QSGM3	0.25	5	60	24
QSGM4	0.5	1	60	24
QSGM5	0.5	5	60	4

[a] Room temperature (20–23 °C).

transferred to dialysis tubes and dialyzed against distilled water for one week to remove any unreacted GM. Finally, the dialyzed solution was lyophilized and stored at −20 °C. Table 1 summarizes the range of conditions used for synthesizing QSGMs with various degree of modifications (DMs).

2.6. Chemical characterization

The success of the proposed modification of QS with GM was evaluated using proton nuclear magnetic resonance (^{1}H NMR) spectroscopy. The spectra of QS and QSGMs were recorded on a Bruker AVANCE II operating at 700 MHz. Approximately 8 mg of each polymer was dissolved in D_2O along with 3.5 mg/mL of SF, which was added as an external reference for quantifying the DM. The chemical composition of both pure and modified polymers was analyzed using Fourier-transform infrared (FTIR) spectroscopy (Spectrum 65, Perkin Elmer, USA) in attenuated total reflectance (ATR) mode. Spectra were recorded over a range of 600 to 4000 cm^{-1}, with a total scan number of 32.

2.7. Gel permeation chromatography

The molecular weight and molecular weight distribution of the samples were analyzed by gel permeation chromatography (GPC) using a Styragel HR column (WAT044228, Waters, USA) and a refractive index (RI) detector (Varian 309-LC). Samples were initially dissolved in water at 10 % (wt./v) by stirring at room temperature, then further diluted to a final concentration of 0.1 wt% and filtered through a 0.2-μm syringe filter prior to injection. Dextran standards were used to create the calibration curve.

2.8. Hydrogel preparation

Hydrogels were prepared from QSGMs by dissolving 0.5 wt./v% of each QSGM (i.e., QSGM1 to QSGM5) and 0.25 wt./v% of LAP as the photoinitiator in water at 50 °C until a transparent solution was obtained. This concentration of LAP was selected based on our previous works with other photosensitive materials such as gelatin methacryloyl (GelMA) (Ajji et al., 2025). The solutions were then exposed to 405 nm blue light from a distance of 5 cm for 60 s to initiate photocrosslinking and hydrogel formation.

2.9. Microstructure imaging

The microstructure of the hydrogels was examined using a scanning electron microscope (SEM, TM3030Plus, Hitachi, Japan). Crosslinked hydrogels were immersed in water for one day, frozen at −20 °C for 24 h, and then lyophilized (FreeZone, Labconco, USA). The lyophilized gels were subsequently fractured under liquid nitrogen to expose their cross-sections. Before SEM imaging, samples were coated with a thin layer of chromium using a Q150R-ES coater (Quorum Technologies, England) to enhance imaging quality.

2.10. Swelling assessment

The swelling capacity of the hydrogels was assessed by immersing them in phosphate-buffered saline (PBS, pH 7.4) at 37 °C for 24 h to reach equilibrium swelling. The swollen hydrogels were then removed from PBS, blotted to remove excess surface water, and weighed. The swelling ratio was calculated by dividing the change in hydrogel weight from the dry to the wet state by the dry weight. The swelling ratio was determined using the following equation:

$$Swelling\ ratio = \frac{W_w - W_d}{W_d} \quad (1)$$

In this formula, W_w is the weight of the swollen hydrogel, and W_d is the weight of the dried hydrogel.

2.11. Mechanical testing

To perform compression tests, QSGM solutions were poured into cylindrical molds (1 cm diameter, 5 mm thickness) and crosslinked as described previously. The gels were then soaked in PBS for 24 h to reach equilibrium. Compression tests were conducted using an HR-2 rheometer (TA Instruments, USA) at 25 °C and 60–80 % relative humidity. Samples were compressed at a rate of 5 mm/min. Each group was tested six times, and stress-strain curves were used to calculate the compression modulus in the linear region.

2.12. Rheological evaluation

Rheological characterization of the polymer solutions was performed using an HR-2 rheometer (TA Instruments, USA) with 15 mm parallel plates. Viscosity vs. shear rate measurements were conducted over a shear rate range of 0.1 to 1000 s^{-1} to investigate the shear-thinning behavior. Additionally, frequency sweep tests were performed within the range of 0.1 to 100 Hz to determine the yield stress, which was defined as the crossover point of the storage and loss moduli. All experiments were conducted at 25 °C with a solution concentration of 0.5 wt%.

2.13. 3D cell encapsulation and cytotoxicity assessment

3T3 mouse fibroblasts were cultured in DMEM-F12 medium supplemented with 10 % fetal bovine serum (FBS) and penicillin-streptomycin antibiotics until 85 % confluency was reached. The cells were then detached from culture flasks using trypsin-EDTA solution, gently spun down, and mixed with polymer solutions at a concentration of 1×10^6 cells/mL. The cell suspension was triturated to ensure homogeneity. A 100 μL aliquot of the cell suspension was pipetted into individual wells of a 48-well cell culture plate and exposed to light for curing. Upon gel formation, culture media was added to the wells and incubated at 37 °C under 5 % CO_2 for two weeks. At designated time points, the plates were removed from the incubator, and the media was discarded. 500 μL of Live/Dead solution was added to each well according to the manufacturer's protocol. The stained hydrogels were then imaged using a SP8-DLS confocal microscope (Leica Microsystems).

2.14. In vitro immune compatibility study

Bone marrow-derived DCs (BMDCs) were differentiated from bone marrow cells isolated from female C57BL/6 mouse femur and tibia as previously described (Colombani et al., 2023; Colombani, Eggermont, Rogers, et al., 2021; Rezaeeyazdi et al., 2022). Briefly, femurs and tibias were harvested, sterilized in 70 % ethanol for 5 min, and washed in PBS several times. Next, epiphysis from both ends of the bone was trimmed, and bone marrow was flushed with PBS (5 mL, 27G needle). Bone marrow cells were dissociated by trituration followed by centrifugation and resuspension in Roswell Park Memorial Institute (RPMI)-1640

medium (Gibco, USA) supplemented with 10 % of heat-inactivated FBS, 100 U/mL of penicillin, 100 μg/mL of streptomycin, 50 μM of 2-mercaptoethanol (ThermoFisher Scientific, USA), and 20 ng/mL of murine GM-CSF (R&D systems, USA). BMDCs were seeded at 1×10^6 cells per mL in low attachment 6-well plates (Corning, USA) and supplemented with additional media with GM-CSF on day 3, followed by replacing half the media with fresh media containing GM-CSF on days 5 and 7. BMDCs were harvested and ready to use on day 10.

To evaluate the DC activation induced by hydrogels, BMDCs were exposed to unmodified QS polymer and QSGM-based hydrogels for 24 h in complete culture media in low attachment 96-well plates (Corning, USA). BMDCs in media alone and 500 ng/mL of lipopolysaccharide (Invivogen, USA) were used as negative and positive controls, respectively. After 24 h, BMDC activation was evaluated by flow cytometry (Attune NxT, ThermoFisher Scientific, USA) using fixable viability dye eFluor506 (ThermoFisher Scientific, USA), TruStain FcX antibody (Clone 93, BioLegend, USA), and the following fluorescent conjugated antibodies: PE/Cyanine7 anti-mouse CD11c Antibody (Clone N418, BioLegend, USA), APC/Cyanine7 anti-mouse I-A/I-E Antibody (Clone M5/114.15.2, BioLegend, USA), MHC Class I (H—2Db) Monoclonal Antibody FITC (Clone 28–14-8, ThermoFisher Scientific, USA), PerCP/Cyanine5.5 anti-mouse CD317 Antibody (Clone 927, BioLegend, USA), Alexa Fluor® 700 anti-mouse CD86 Antibody (Clone GL-1, BioLegend, USA), BV650 Rat Anti-Mouse CD40 (Clone 3/23, BD Biosciences, USA), PE anti-mouse CD70 Antibody (Clone FR70, BioLegend, USA), Brilliant Violet 421™ anti-mouse CD197 (CCR7) Antibody (Clone 4B12, BioLegend, USA). Supernatants were collected from the wells, and pro-inflammatory cytokines were quantified using Mouse IL-6 DuoSet ELISA and Mouse TNF-alpha DuoSet ELISA (R&D systems, USA).

2.15. 3D printing

3D printing of QSGM1 (representative of the synthesized polymers) was performed using a BIO X6 bioprinter (CELLINK, USA). A 0.5 % solution of QSGM1 was prepared as described earlier. The solution was then poured into the printing cartridge, which was fitted with a 30 G blunt needle (nominal ID: 0.159 mm), and loaded into the bioprinter. The printing conditions were as follows: printing pressure of 25 kPa, cartridge temperature of 5 °C, and printing speed of 5 mm/s. The G-codes required for printing were generated using DNAStudio software (CELLINK) based on the available STL files. 3D printing was performed within a supporting bath made of Carbopol ETD 2020. Briefly, Carbopol powder was prepared in water at a 1 % concentration overnight. The pH was adjusted to 7.1 using 5 M NaOH, which increased the solution's viscosity to form a gel-like suspension. The Carbopol gel was degassed by centrifugation and loaded into Petri dishes for printing. After 3D printing in the supporting bath, the printed constructs were crosslinked by exposure to visible blue light (405 nm) for 1 min, as described in Section 2.6. Printing fidelity (Pr) was quantified using the following equations (Ouyang et al., 2016):

$$Pr = \frac{\pi}{4C} \tag{2}$$

$$C = \frac{4\pi A}{L^2} \tag{3}$$

In these equations, C is circularity, A is the area, L is the perimeter, and Pr is printing fidelity.

2.16. Statistical analysis

All tests were conducted in triplicate. Statistical analysis of the results was performed to determine the significance of the differences. p-Values <0.05 were considered statistically significant. P-values were categorized into four levels: *p < 0.05, **p < 0.01, ***p < 0.001, and ****p < 0.0001.

3. Results and discussion

3.1. Physicochemical characterization of QS and QSGM

We used GM to modify QS, producing photosensitive QSGM (Fig. 1a). GM is considered more efficient than methacrylic anhydride (MA), as MA can undergo hydrolysis when incorporating methacrylates onto polymer backbones (Di Muzio et al., 2022). In an acidic environment, GM will react with the hydroxyl or carboxylic acid pendant groups on the QS backbone through epoxide ring opening, introducing reactive vinyl bonds to QS (Reis et al., 2009). Different reaction conditions were investigated to formulate QSGMs with various DMs, and the sample coding is summarized in Table 1. QS was extracted from quince seeds, yielding 12.03 ± 1.46 %. To better understand the structure and composition of the QS polysaccharide, we first used GC–MS with chemical derivatization to convert carbohydrates into volatile TMS methyl glycosides. The retention times and fragmentation patterns of each peak in the GC chromatogram were analyzed using standards to identify the sugar components in the derivatized biopolymer (Supplementary Fig. S1). GC–MS analysis revealed the presence of rhamnose (Rha), ribose (Rib), arabinose (Ara), fucose (Fuc), xylose (Xyl), glucuronic acid (GlcA), galacturonic acid (GalA), mannose (Man), galactose (Gal), and glucose (Glu) in QS. The monosaccharide composition and their molar percentages are summarized in Table 2. The composition shows that xylose (65.6 mol%) is the major saccharide, followed by glucose (15.1 %), arabinose (9 %), and galactose (6.3 %), with minor amounts of other monosaccharides. Uronic acid accounts for 2.5 mol%. Additionally, total carbohydrates make up 48 % of the dry weight of the extracted sample.

Further structural analysis of QS was conducted using methylation, a powerful tool for elucidating the structure of polysaccharides (Laine et al., 2002). In the initial step, the acidic polysaccharide undergoes reduction to achieve a neutral state. After reduction, all free hydroxyl (OH) groups within the polysaccharide are methylated. The resultant per-methylated polysaccharide then undergoes a sequence of hydrolysis, reduction, and acetylation processes to yield partially methylated alditol acetates (PMAAs), which are subsequently analyzed through GC–MS. Using standard data from the Complex Carbohydrate Research Center (University of Georgia, USA) Spectral Database for PMAA, the methylation analysis results of QS revealed a complex structure with diverse linkage patterns (Table 3 and Supplementary Fig. S2).

In both composition and linkage analyses, xylose was the predominant residue. The xylose residues appear as (1 → 4)- and (1 → 2, 4)/(1 → 3, 4)-linked xylopyranosyls at molar ratios of 16.4 % and 30 %, respectively, indicating that QS has highly branched polysaccharides. Six branching points were identified in the sample, specifically 2,4-Xyl, 3,4-Xyl, 3,4-Glc, 2,4-Glc, and 4,6-Man. The major non-reducing terminal residue was T-Ara, accounting for 3.8 %, followed by T-Glc (2.4 %), T-Gal (1.4 %), and T-Xyl (1.2 %).

Linkage results for rhamnose, ribose, fucose, and uronic acid were not characterized, as these sugars were present in very low amounts (<1 %). Based on the results of monosaccharide composition and glycosidic linkage analysis, one predicted structure of the QS polysaccharide is a xylan (1,4-Xyl) backbone with branching at the O-2 or O-3 positions, involving arabinose, galactose, glucose, and minor amounts of GalA and GlcA.

To confirm the reactions, we first used ATR-FTIR to identify the main functional groups in the extracted QS and modified QSGM polymers. For QS, the resulting spectrum (Fig. 1b) showed a broad peak at 3346 cm^{-1}, characteristic of hydroxyl groups and hydrogen bonding (Jafari et al., 2019). Other characteristic peaks of QS were observed at 2920, 1602, 1419, 1378, and 1046 cm^{-1}, corresponding to CH stretching, carbonyl (C=O) asymmetric stretching, C═O symmetric stretching, carboxyl, and C—O groups, respectively (Ashraf et al., 2018; Guzelgulgen et al., 2021). After modifying QS with GM, a shoulder appeared at 1637 cm^{-1}, indicating the C═C bond of the grafted GM (Guilherme et al., 2005). The

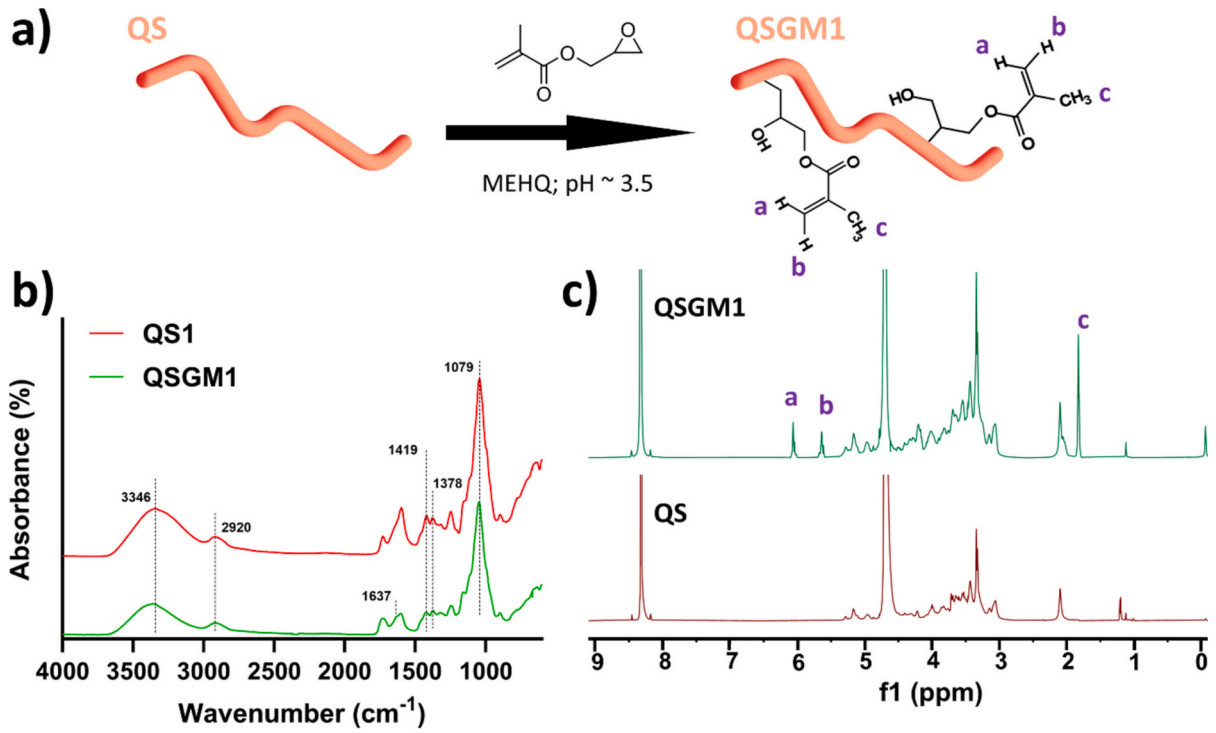

Fig. 1. Synthesis and characterization of QSGM. (a) Schematic representation of reaction between QS and GM. (b) FTIR spectra of extracted QS and QSGM1 and (c) ^{1}H NMR spectra of QS (bottom row) and QSGM1 (top row) in D_2O.

Table 2
Monosaccharide composition of QS.

Glycosyl residues	Quince seed extract (mol%)
Ribose (Rib)	0.7
Arabinose (Ara)	9.0
Rhamnose (Rha)	0.5
Glucose (Glc)	15.1
Fucose (Fuc)	0.2
Xylose (Xyl)	65.6
Glucuronic acid (GlcA)	1.9
Galacturonic acid (GalA)	0.5
Mannose (Man)	0.2
Galactose (Gal)	6.3
Total	100

Table 3
Relative percentages of linkage residues detected in the quince seed extract.

Retention time (min)	Linkage residue	Percent area (mol %)
11.865	Terminal arabinopyranosyl (t-Ara)	3.8
12.109	Terminal xylopyranosyl (t-Xyl)	1.2
13.661	Terminal glucopyranosyl (t-Glc)	2.4
14.494	Terminal galactopyranosyl (t-Gal)	1.4
14.990	4-Linked arabinopyranosyl (4-Arap)	0.5
15.087	3-Linked arabinopyranosyl (3-Arap)	0.2
15.755	4-Linked xylopyranosyl (4-Xyl)	16.4
16.454	3-Linked glucopyranosyl (3-Glc)	0.4
17.072	4-Linked mannopyranosyl (4-Man)	0.1
17.640	6-Linked glucopyranosyl (6-Glc)	4.5
18.040	4-Linked galactopyranosyl (4-Gal)	28.4
18.723	2,4 + 3,4-linked xylopyranosyl (2,4/3,4-Xyl)	30.0
18.991	6-Linked galactopyranosyl (6-Gal)	4.4
19.759	3,4-Linked glucopyranosyl (3,4-Glc)	0.9
19.867	2,4-Linked mannopyranosyl (4-Man)	0.8
20.358	2,4-Linked glucopyranosyl (2,4-Glc)	0.8
20.438	4,6-Linked mannopyranosyl (4,6-Man)	0.8
20.921	2,6-Linked glucopyranosyl (2,6-Glc)	0.2
21.410	4,6-Linked glucopyranosyl (4,6-Glc)	11.1
23.55	3,4,6-Linked glucopyranosyl (3,4,6-Glc)	0.3

presence of the shoulder became more pronounced with higher GM concentrations, indicating higher degrees of modification (Supplementary Fig. S3). Additionally, post-modification, the peak ratios between 1420 and 1380 cm^{-1} shifted, with the intensity of the peak around 1420 cm^{-1}, initially greater, becoming lower than that of the peak around 1380 cm^{-1}. This change further confirms the occurrence of the reaction.

Further investigations into the synthesis of QSGM were conducted using ^{1}H NMR. Fig. 1c shows the NMR spectra of QS and QSGM1. The 1D spectra display characteristic peaks typical of polysaccharides, representing the various monosaccharides present in the polysaccharide backbone (Wang et al., 2017). The diagnostic anomeric chemical shifts in the region from 4.5 to 5.5 ppm revealed different configurations of glycosidic bonds: the α-configuration appears at >4.7 ppm, while the β-configuration appears at <4.7 ppm. The non-anomeric sugar skeleton protons appeared around 3.4 to 4.4 ppm, and the acetyl protons appeared between 2.2 and 1.8 ppm. Based on the QS spectra, further purification was not needed, as the sample primarily contained carbohydrates with minor other components (proteins, lactate).

The absence of peaks between δ 6–8 ppm indicated no presence of phenols or ferulic acid. Peaks around 1.1 ppm were attributed to branched and unbranched methyl group links of rhamnose. An intense peak at 2.1 ppm suggested a high degree of acetylation in the extracted sample. According to the literature, the sharp doublet around ~1.2 ppm could tentatively be assigned to lactate (Lockett et al., 1996). Minor amounts of water-soluble proteins may be present in the sample. Due to the linkage diversity, the spectrum peaks overlapped in the resonance region (5.4–4.4 ppm), making them difficult to assign.

The QSGM spectra for all synthesized groups showed similar characteristic peaks to the QS spectrum (Supplementary Fig. S4), confirming that QSGM remains largely intact during the reaction, with all characteristic monosaccharide and glycosidic bonds appearing at similar ppm values. Therefore, the overall chemical structures of QS and QSGM are very similar. However, the spectrum of QSGM1 displays three new

distinctive peaks: the peak at δ = 1.8 ppm is attributed to the methyl protons of GM, and the two peaks at δ = 5.6 and 6.1 ppm correspond to the vinyl carbon-linked hydrogens (Bencherif et al., 2008). These new peaks confirm the formation of QSGM. However, different groups exhibited varying peak intensities, indicating differences in the degree of modification (DM) (Supplementary Fig. S4). To quantify these differences, SF was added as an external reference. Since the structure of QS is not extensively studied or well-known, calculating the degree of substitution is challenging. Instead, the use of SF facilitates the calculation of DM. The peak of SF appears around δ = 8.3 ppm, well-separated from the recorded peaks of pure QS and modified QSGMs, allowing for quantification of the degree of modification.

The integration of the SF peak (at δ = 8.3 ppm) and the vinyl carbon-linked hydrogens (at δ = 5.6 and 6.1 ppm) was used to measure DM. Knowing the amounts of SF and QSGMs in the solutions, along with the molecular weight of QSGM from the GPC test, enabled us to calculate DM using the integration values (Table 4). The degree of modification was found to range from 65.95 ± 4.07 to 214.29 ± 2.79 mmol of GM per mmol of polymer, with QSGM1 having the highest DM and QSGM4 showing the lowest. As expected, an increased GM/QS ratio, reaction time, and reaction temperature resulted in higher DMs.

The molecular weight distributions of QS and QSGM1 were determined using GPC chromatograms to quantify the DM (Supplementary Fig. S5 and Supplementary Table S1). The data showed two distinct peaks on GPC, indicating that the polysaccharide has two molecular weight distributions: 29.6 ± 0.3 kDa and 912 ± 3 kDa. For QSGM1, two peaks were also observed, but the molecular weights shifted to 24 ± 0.8 kDa and 842 ± 6 kDa. This reduction may be attributed to the slight degradation of QS during the chemical reaction.

3.2. Swelling properties

The equilibrium swelling of hydrogels was measured to examine the effects of various reaction conditions on the crosslinking density of the prepared hydrogels. Due to the low concentration of QSGM solutions used for hydrogel formation (0.5 wt%), all samples showed high swelling ratios, ranging from 320 to 580 g/g (Fig. 2a). Specifically, the swelling ratios were 323.8 ± 3.8, 511.4 ± 29.6, 407.6 ± 4.3, 578.3 ± 38.0, and 464.3 ± 28.1 g/g for QSGM1, QSGM2, QSGM3, QSGM4, and QSGM5, respectively. It is noteworthy that the chosen swelling medium, PBS, contains charged cations that interact with the polymer backbone, leading to decreased osmotic pressure and, consequently, a reduced swelling percentage compared to salt-free media like water (Zhao et al., 2006). Additionally, samples with higher degrees of GM modification on the QS backbone were observed to have lower swelling ratios. A higher degree of modification (DM) has been associated with increased crosslinking density, as previously reported (Velasco-Rodriguez et al., 2021). This result was expected, as higher GM modification indicates more available reaction sites on the QS backbone. Consequently, there is an increased likelihood of successful connections between polymer chains, leading to the formation of a denser 3D network. This denser structure restricts backbone movement and reduces swelling (Bencherif et al., 2008; Y. Chen et al., 2020). The crosslinking density within hydrogels can be quantified using the swelling method, as described previously (Huang et al., 2019), however, this analysis was beyond the scope of the current work.

Table 4
DM of synthesized QSGMs calculated based on ^{1}H NMR.

Sample code	DM (mmol of GM per mmol of polymer)
QSGM1	214.29 ± 2.79
QSGM2	67.62 ± 4.05
QSGM3	145.90 ± 11.70
QSGM4	65.95 ± 4.07
QSGM5	135.25 ± 7.71

3.3. Microstructure analysis

The morphology of the freeze-dried hydrogels was examined using SEM. Fig. 2b–f shows the highly porous microstructure of the hydrogels, characterized by microsized interconnected pores and thin pore walls. Overall, the microstructures of the hydrogels are similar, with some differences in pore orientation and size. However, as these parameters can be influenced by the preparation process (e.g., freezing and subsequent lyophilization), it is not possible to directly associate these variations with crosslinking density (Annabi et al., 2010; De France et al., 2018). While these pores do not precisely replicate the actual size of pores in a swollen hydrogel, they may indicate that the hydrogels could facilitate nutrient and oxygen penetration, as well as exchange, potentially supporting cell migration and infiltration toward the inner regions of the gel (Lantigua et al., 2020).

3.4. Mechanical and rheological properties

Further investigation into the effect of DM on the properties of the fabricated hydrogels was conducted using an unconfined compression test. The mechanical properties of the scaffolds, including modulus and stiffness, are known to influence cellular behavior (Su et al., 2022). The results of the compression test are shown in Fig. 3. The data indicate that hydrogels with a higher degree of modification are stiffer, and able to bear higher loads and compressions. This increased stiffness is attributed to a higher degree of crosslinking after exposure to visible light, creating a more rigid matrix that effectively distributes applied stress throughout the hydrogel. Additionally, the calculated compressive moduli ranged from 0.6 ± 0.1 to 1.2 ± 0.3 kPa, with QSGM1 exhibiting the highest value. For context, human tissues display varying biomechanical properties, from under 1 kPa for soft tissues to several GPa for hard tissues (Budday et al., 2020; Handorf et al., 2015). As a result, it is critically important to tailor the mechanical properties of the hydrogels, along with other characteristics, to match the requirements of the targeted tissue. Based on our results, the mechanical properties of the fabricated hydrogels are suitable for tissue engineering applications involving soft tissues such as adipose tissue and nerves. Therefore, we hypothesize that increasing the QSGM concentration could enable the hydrogels to achieve stiffness levels suitable for other soft tissues, including muscle and cardiac tissues.

Rheological characteristics such as shear-thinning properties and yield stress are among the most critical properties for materials intended for 3D (bio)printing. Following the successful modification of QS with methacrylate groups, which allow for photocrosslinking, we investigated the effect of DM on the rheological behavior of the polymeric (bio) ink. The shear-thinning behavior of the inks was analyzed by recording changes in viscosity at different shear rates (Fig. 4a and b). All (bio)inks, including unmodified QS, exhibited shear-thinning behavior within the tested range. Additionally, we applied the power-law equation to the results to determine the shear-thinning index (n). According to the power-law model, an index of $n > 1$ indicates shear-thickening behavior, while $n < 1$ is characteristic of shear-thinning materials (Schwab et al., 2020). The results indicated that for all samples, n values ranged from 0.33 to 0.36, confirming their shear-thinning behavior. During 3D (bio) printing, particularly in extrusion-based approaches, the (bio)ink is subject to shear stresses due to flow. Shear-thinning properties can significantly reduce the shear experienced by the (bio)ink during printing, thereby facilitating the printing process (Schwab et al., 2020).

Next, we used amplitude sweep measurements to investigate the yield stress of the (bio)inks. As shown in Fig. 4c–h, at stresses below 3 Pa, the (bio)inks remained in the linear viscoelastic (LVE) region, with the modulus remaining nearly constant. Additionally, all (bio)inks displayed a higher storage modulus (G') than loss modulus (G") in this region, indicating a more gel-like behavior. Yield stresses were calculated at the crossover point of G' and G". Similar to the shear-thinning behavior, the yield stresses were consistent across samples, ranging

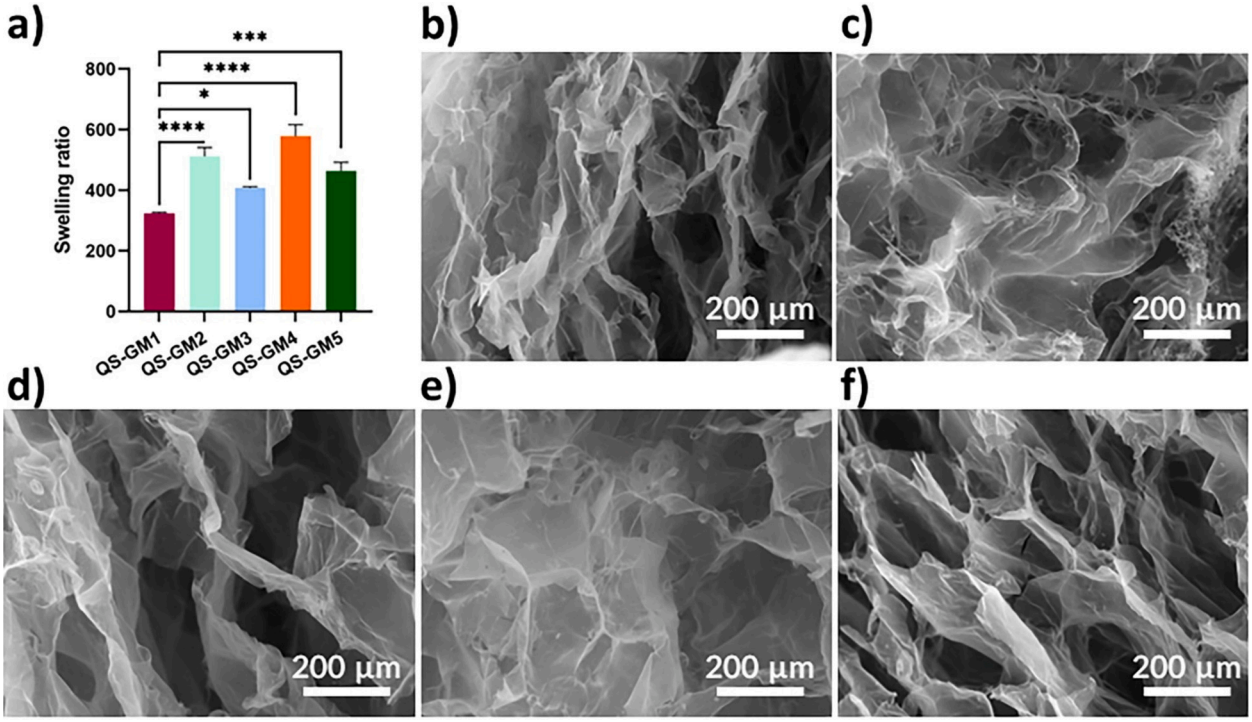

Fig. 2. Characterization of the physical properties of QSGMs. (a) Equilibrium swelling ratio of different QSGM hydrogels. SEM micrographs showing the cross-sectional morphology of (b) QSGM1, (c) QSGM2, (d) QSGM3, (e) QSGM4, and (f) QSGM5. Images were captured at 180× magnification. (*$p < 0.05$, ***$p < 0.001$, and ****$p < 0.0001$).

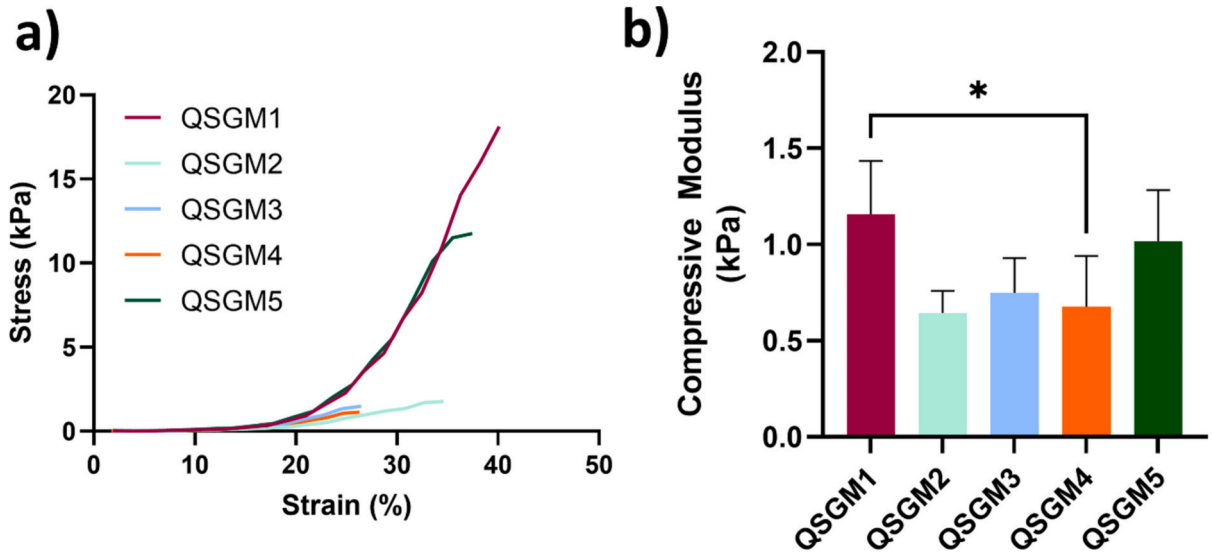

Fig. 3. Evaluating the mechanical properties of the QSGMs. (a) Representative unconfined compressive strain/stress curves of fabricated hydrogels and (b) calculated compressive modulus for fabricated hydrogels. (*$p < 0.05$.)

from 3 to 4 Pa. These low yield stresses suggest that the (bio)inks possess easy flowability. Overall, the results indicate that modification of QS with GM did not significantly alter the rheological properties.

3.5. Cell encapsulation and viability

The potential application of QSGMs for tissue engineering was explored by assessing cell encapsulation in QSGM1, the polymer with the highest DM. Live/dead staining of encapsulated cells was performed to evaluate the cytocompatibility of the hydrogels (Fig. 5, and Supplementary Videos S1–S6). As shown in Fig. 5b and c, most cells remained viable over the entire 2-week period. Staining conducted immediately after crosslinking indicated that the process did not lead to excessive cell death. The LAP concentration can affect the hydrogels' crosslinking efficacy, which can change their physical and mechanical properties. While we did not investigate the effect of LAP concentration on hydrogel properties, at 0.25 % LAP concentration, we saw no adverse effects on cell viability. Although this concentration of LAP may be excessive, it did not harm the encapsulated cells and ensured the formation of a hydrogel upon exposure to light. Compared to more conventional UV curing of photosensitive hydrogels, using a visible light-activated photoinitiator (LAP) and blue light at a wavelength of 405 nm can

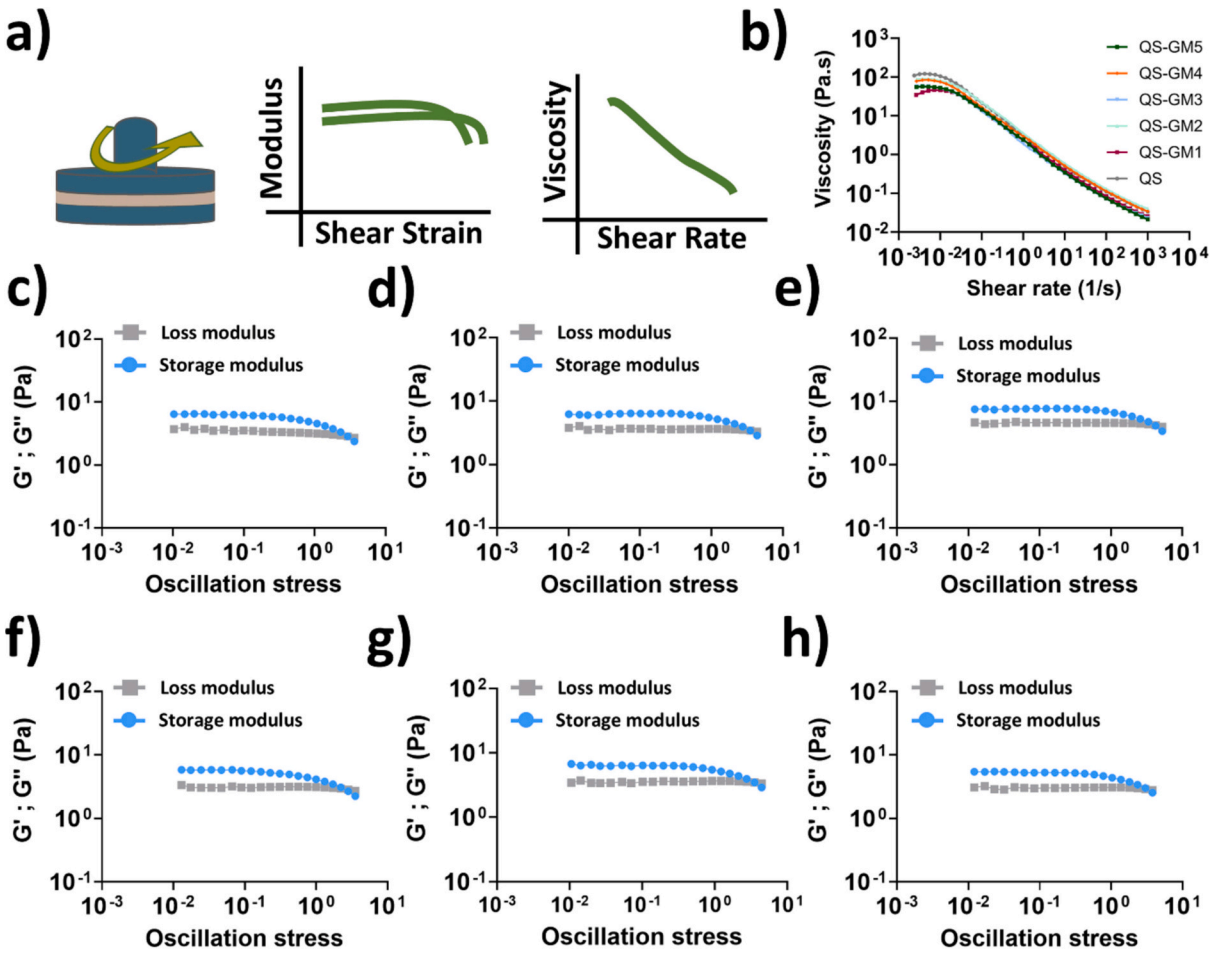

Fig. 4. (a) Rheological behavior of QS and QSGMs. (b) Viscosity vs. shear rate for formulated inks showing the shear-thinning properties of the (bio)inks. Amplitude sweeps tests showing the LVE region and crossover of storage and loss modulus (yield stress) for (c) QS, (d) QSGM1, (e) QSGM2, (f) QSGM3, (g) QSGM4, and (h) QSGM5.

significantly reduce the adverse effects of UV irradiation on cells (Yu et al., 2020). The extended incubation period of cell encapsulation within QSGM1 hydrogels did not significantly affect cell survival, indicating that modified QSGM1 did not exhibit notable cytotoxicity. Furthermore, since QSGM1 has the highest DM, other synthesized QSGMs with lower DMs are expected to exhibit similar cytocompatibility. However, it is noteworthy that cells displayed a rounded morphology at early time points, likely due to the absence of cell-binding motifs and spatial restrictions. QS is a polysaccharide, and, like most polysaccharides such as alginate, lacks cell-binding motifs on its backbone (Firipis et al., 2022). However, by day 14, some cells at the gel's border exhibited an elongated morphology, typical of fibroblasts. This could be attributed to the deposition of extracellular proteins by the cells, enhancing their attachment and elongation. Given that QSGM is soluble in cell culture media and that QSGM hydrogels successfully supported cell encapsulation with minimal cytotoxicity, developing bioinks and conducting 3D bioprinting with these materials would be feasible in future studies.

3.6. Activation of BMDCs by QSGM hydrogels

Biomaterials can induce a foreign-body response at the local site, leading to severe inflammation, tissue impairment, and the formation of fibrotic capsules. This response can hinder further host interaction, result in rejection, and ultimately cause loss of function (Adusei et al., 2021; Christo et al., 2015). Dendritic cells (DCs) play a crucial role in initiating the innate immune response and priming the adaptive immune response against foreign biomaterials (Abdullah et al., 2020; Bhatt et al., 2022). Understanding the interaction between QSGM hydrogels and DCs is crucial for predicting biocompatibility, an essential feature for tissue engineering applications. Therefore, the immunogenicity of QSGM hydrogels was evaluated by assessing the activation state of DCs and monitoring their pro-inflammatory cytokine secretion profile to ensure that these hydrogels do not trigger undesirable immune responses.

BMDCs were cultured in the presence of QS polymer and QSGM hydrogels for 24 h. The upregulation of co-stimulatory and activating receptors, including CD86, CD317, MHC I, MHC II, and CCR7, on CD11c+ DCs was assessed using flow cytometry (Fig. 6a–e, Supplementary Fig. S5, and Supplementary Table S2). Additionally, the secretion of pro-inflammatory cytokines such as IL-6 and TNF-α was measured via ELISA (Fig. 6f–g and Supplementary Table S2).

Compared to untreated BMDCs, QS polymer and QSGM hydrogels did not upregulate the expression of CD86, MHC I, MHC II, and CCR7 as observed with LPS treatment. On the contrary, the expression of CD86 and MHC II was slightly downregulated with QS (7.7 ± 1.2 % for CD86, 15.5 ± 1.0 % for MHC II) and QSGM (QSGM1: 6.9 ± 0.4 % for CD86, 15.5 ± 0.4 % for MHC II; QSGM4: 6.3 ± 0.5 % for CD86, 15.4 ± 0.7 % for MHC II) compared to the media control (10.3 ± 0.8 % for CD86, 17.7 ± 0.1 % for MHC II).

However, unmodified QS polymer led to a slight upregulation of CD317 (10.8 ± 5.1 %) on BMDCs compared to the media control (4 ± 0.2 %), though the levels remained significantly lower than the positive control (LPS) (64 ± 1 %). In contrast, QSGM hydrogels did not show a significant change in CD317 levels (6.9 ± 1 % for QSGM1 and 7.0 ± 1.2

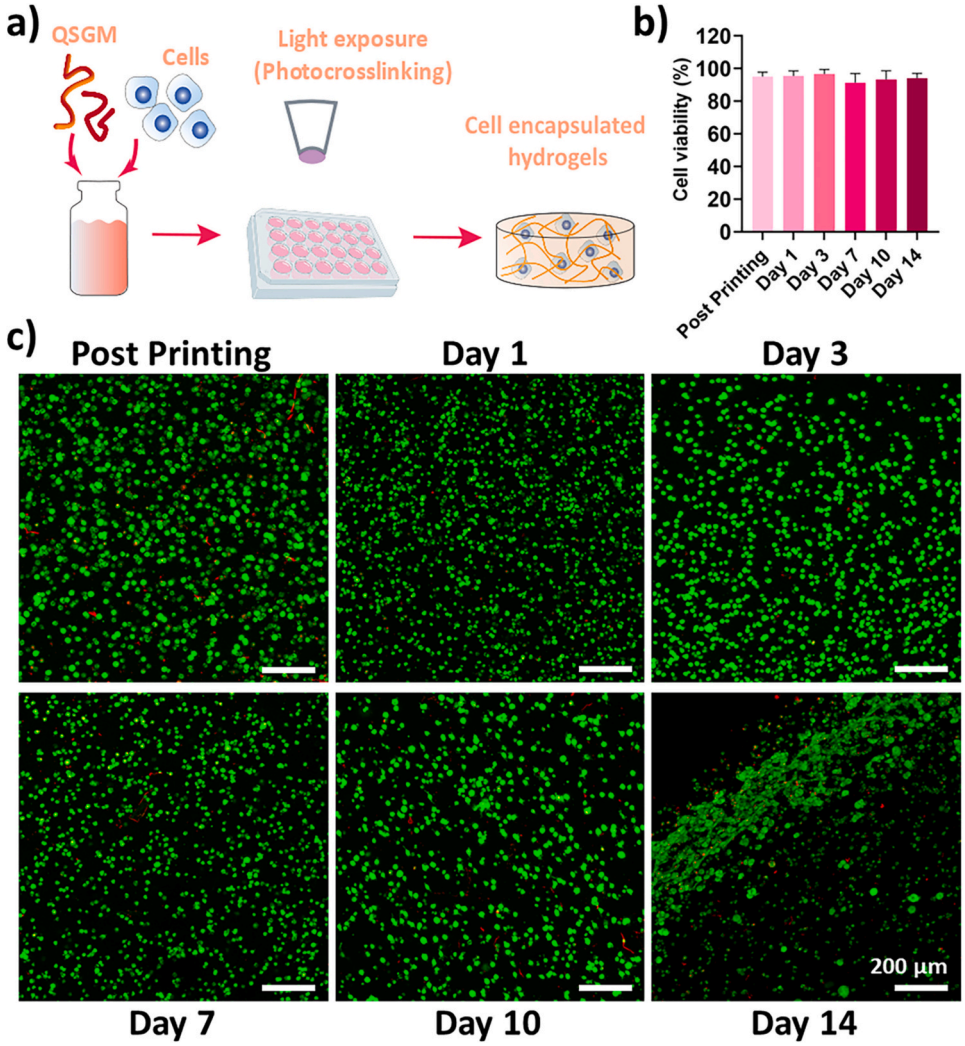

Fig. 5. 3D cell encapsulation and in vitro evaluation of cell cytotoxicity of QSGMs. (a) Fibroblast cells were mixed with the hydrogel precursor and exposed to 405 nm light to form the gels. (b) Quantification of cell viability based on live/dead staining images, and (c) maximum intensity projection of live/dead fluorescent staining showing live (green) and dead (red) fibroblasts being encapsulated in QSGM1 hydrogel over two weeks of cell culture. (Scale bar = 200 µm.)

% for QSGM4).

While QS polymer triggered the secretion of IL-6 (18,012 ± 20,249 pg/mL) and TNF-α (2,269 ± 2346 pg/mL) by BMDCs, QSGM hydrogels did not substantially elevate pro-inflammatory cytokine secretion ($p > 0.05$). This effect may be attributed to changes in surface charge following QS polymer modification to QSGM, as well as differences in the modes of contact between dissolved QS polymer and QSGM hydrogel with BMDCs (S. Wang et al., 2022). Overall, our findings demonstrate that QSGM hydrogels do not significantly activate BMDCs, as indicated by the lack of upregulation in activation markers (CD86, MHC I, MHC II, and CCR7) and the minimal secretion of pro-inflammatory cytokines (IL-6, TNF-α) compared to untreated controls. This is in contrast to the response induced by lipopolysaccharide (LPS), a potent immunostimulant used as a positive control in our study. These results suggest that QSGM hydrogels have a lower immunogenic potential compared to more traditional biomaterials, such as collagen, fibrin, and gelatin, which are known to elicit a stronger immune response (Koyyada & Orsu, 2021; Qi et al., 2018). Additionally, limited evidence suggests that quince seed-derived biomaterials cause significant inflammatory reactions. Most studies indicate that quince seed mucilage-based scaffolds possess beneficial properties, including anti-inflammatory effects and biocompatibility (Guzelgulgen et al., 2021; Hussain et al., 2019; Şimşek et al., 2020; Yilmaz et al., 2023). Thus, the ability of QSGM hydrogels to interact with the immune system without triggering a strong inflammatory response makes them promising candidates for various biomedical applications, including wound healing, drug delivery, and tissue regeneration.

Future research should assess the long-term immunogenicity of QSGM hydrogels in vivo to confirm whether they retain their low immunogenic profile over extended periods, as chronic exposure may provoke different immune responses. Employing relevant animal models will help translate these findings into clinical applications. Furthermore, investigating the effects of surface modifications and functionalization on QSGM hydrogels could enhance their biocompatibility by affecting protein adsorption, cell adhesion, and immune cell interactions, thereby improving their performance in specific applications. In conclusion, our study highlights the potential of QSGM hydrogels as suitable biomaterials for tissue engineering, offering low immunogenicity and promising biocompatibility.

3.7. 3D printing

As proof of concept, QSGM1 was utilized to explore the feasibility of utilizing this polysaccharide with additive manufacturing techniques to print 3D tissue-engineered scaffolds. Initially, we attempted to print QSGM1 in air. However, due to its low viscosity and yield stress at this

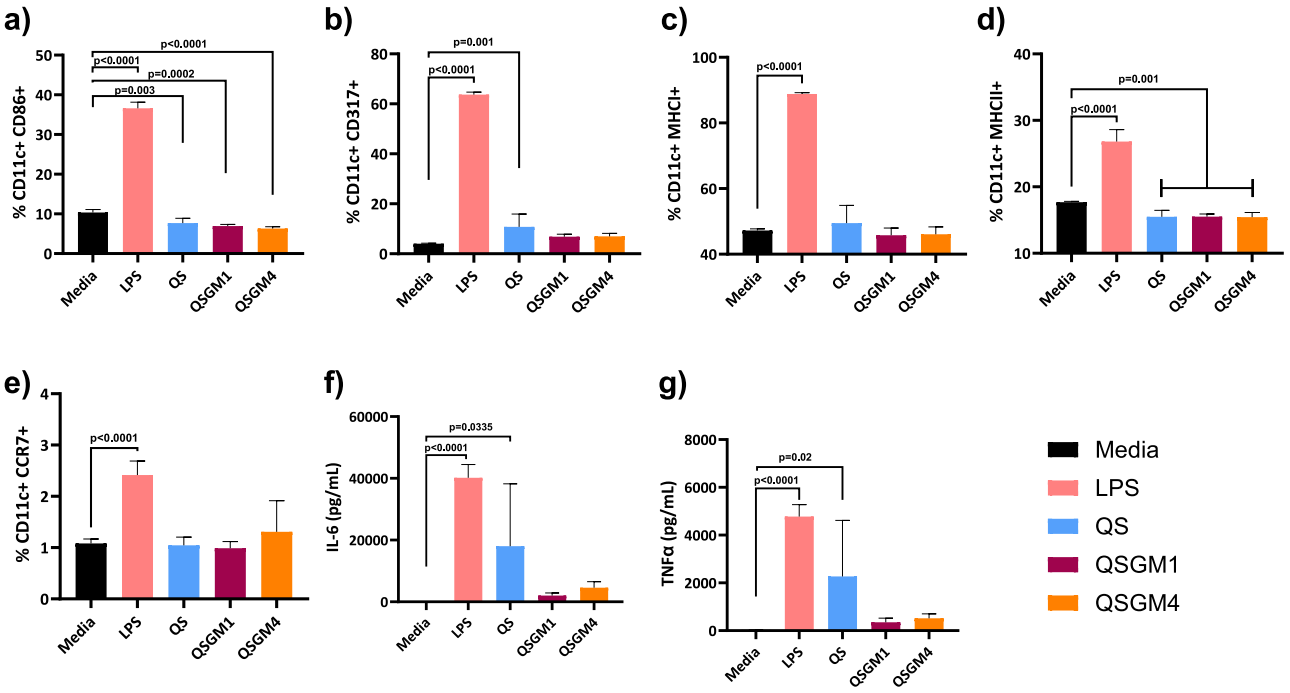

Fig. 6. Activation of mouse bone-marrow-derived dendritic cells (BMDCs) in vitro. BMDCs were cultured for 24 h in in the following stimulating conditions: Media (negative control), LPS (Lipopolysaccharide) at 500 ng/mL (positive control), QS polymer, QSGM1, and QSGM5. Fraction of activated BMDCs (a) CD11c+ CD86+ (b) CD11c+ CD317+ (c) CD11c+ MHCI+ (d) CD11c+ MHCII+ (e) CD11c+ CCR7+ 24 h after culture with different conditions. Concentration of secreted (f) IL-6 (g) TNFα in the BMDC culture supernatant upon stimulation with different conditions. Values represent mean and SD (n = 5). Data of the stimulating conditions were compared to media control and analyzed using one-way analysis of variance (ANOVA) and Tukey's post hoc test using GraphPad software.

concentration, as indicated by rheological analysis, the 3D-printed constructs collapsed without additional support. Therefore, we used a support bath, which has been shown to facilitate the printing of low-viscosity (bio)inks (Lee et al., 2019). The support bath effectively compensates for the low yield stress of the (bio)ink, preventing the printed filaments from collapsing (Savoji et al., 2020). Using this approach and Carbopol ETD 2020 as the support bath, we successfully 3D-printed various structures. These included a lattice/mesh cube with a 1 cm side, demonstrating the feasibility of 3D printing both simple and complex structures with the developed (bio)inks (Fig. 7 and Supplementary Fig. S6). For optimal printing, the constructs should closely match the initial design and maintain their structure until further treatment and crosslinking of the printed hydrogel (Schwab et al., 2020). In our experiments, the printed scaffolds demonstrated high printing fidelity, with minimal compromise or distortion of the lattice/mesh structure and porosity across multiple layers. The calculated printing fidelity (Pr), determined using Eqs. (2) and (3), was 0.90 ± 0.15. Additionally, high shape retention was observed during the printing of both straight and curved constructs, indicating the potential of the developed system for 3D (bio)printing of more complex structures.

4. Conclusions and future directions

In this study, we designed and developed for the first time, photosensitive polymers derived from naturally occurring QS mucilage. QS was successfully modified with GM to introduce pendant vinyl groups capable of undergoing radical polymerization in the presence of an appropriate photoinitiator and light source. A systematic examination of reaction conditions indicated that the QS-to-GM ratio had the most significant impact on the final degree of modification (DM). Hydrogels were formed using the resulting products (QSGMs) in the presence of LAP and a 405 nm wavelength light source. These QSGM-based hydrogels exhibited high swelling capacity and a compressive modulus suitable for soft tissue engineering applications. Furthermore, the modification did not significantly alter the rheological properties of QS, preserving its strong shear-thinning behavior and maintaining rheological properties suitable for 3D (bio)printing.

Moreover, we demonstrated that QSGM is highly promising for additive manufacturing and 3D (bio)printing applications. Cellular analyses further revealed that QSGM hydrogels did not significantly activate BMDCs and supported the sustained viability of encapsulated cells over time. Overall, our results confirm the potential of QSGM as a novel material for fabricating tissue-engineered scaffolds.

To further expand the application of this innovative photosensitive material in soft tissue engineering, it could be combined with other photosensitive materials, such as GelMA, to create new bioinks with enhanced bioactivity and tailored mechanical properties. This approach could support the 3D bioprinting of complex structures, including muscle and cardiac tissues.

Supplementary data to this article can be found online at https://doi.org/10.1016/j.carbpol.2024.123140.

CRediT authorship contribution statement

Arman Jafari: Writing – original draft, Visualization, Validation, Software, Methodology, Investigation, Formal analysis, Conceptualization. **Khushbu Bhatt:** Writing – review & editing, Investigation, Formal analysis. **Seyyed Vahid Niknezhad:** Writing – review & editing, Conceptualization. **Abdellah Ajji:** Writing – review & editing, Resources. **May Griffith:** Writing – review & editing, Resources. **Gregor Andelfinger:** Supervision. **Sidi A. Bencherif:** Writing – review & editing, Validation, Resources, Funding acquisition. **Houman Savoji:** Writing – review & editing, Supervision, Resources, Funding acquisition, Conceptualization.

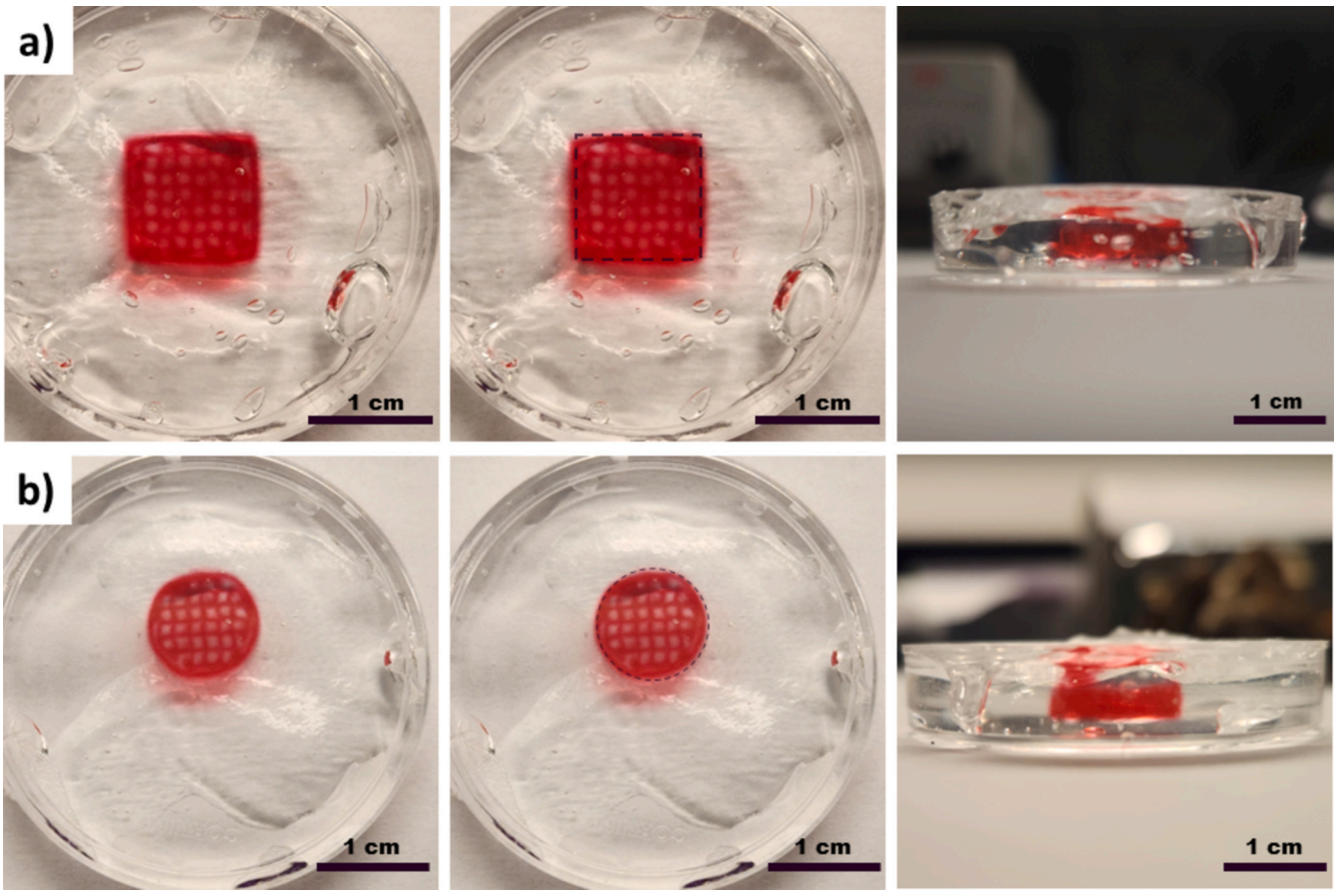

Fig. 7. Samples of different 3D printed QSGM-based hydrogel constructs. (a) 1 × 1 × 0.5 cm^3 cube and (b) Ø 1 cm, 0.5 cm thickness cylindrical structures using QSGM1 in a supporting bath. Dashed areas in the middle images show the perimeter of the CAD design.

Declaration of competing interest

The authors declare that they have no known competing financial interests or personal relationships that could have appeared to influence the work reported in this paper.

Acknowledgments

Our work is supported by the Natural Sciences and Engineering Research Council of Canada, Discovery Grant (NSERC, RGPIN-2021-03960), Fonds de Recherche du Québec - Santé (FRQS) Research Scholar J1, Montreal TransMedTech Institute (iTMT), and CHU Sainte-Justine Research Center (CRCHUSJ) of the University of Montreal. A.J. gratefully acknowledges the FRQS Doctoral Scholarship and the Merit Scholarship from the Faculty of Medicine at the University of Montreal. S.A.B. gratefully acknowledges financial support from the National Institutes of Health (NIH, 1R01EB027705) and the National Science Foundation (NSF CAREER, DMR 1847843). M.G. acknowledges support from her CIHR Canada Research Chair and Caroline Durand Foundation Research Chair. The chemical composition of QS was analyzed by the Complex Carbohydrate Research Center (CCRC) at the University of Georgia, supported by the U.S. Department of Energy, Office of Science, Basic Energy Sciences, Chemical Sciences, Geosciences, and Biosciences Division, under award #DE-SC0015662.

Data availability

Data will be made available on request.

References

Abdullah, T., Bhatt, K., Eggermont, L. J., O'Hare, N., Memic, A., & Bencherif, S. A. (2020). Supramolecular self-assembled peptide-based vaccines: Current state and future perspectives. *Frontiers in Chemistry, 8*, Article 598160.

Adusei, K. M., Ngo, T. B., & Sadtler, K. (2021). T lymphocytes as critical mediators in tissue regeneration, fibrosis, and the foreign body response. *Acta Biomaterialia, 133*, 17–33.

Ahmad, Z., Salman, S., Khan, S. A., Amin, A., Rahman, Z. U., Al-Ghamdi, Y. O., … Khan, S. B. (2022). Versatility of hydrogels: From synthetic strategies, classification, and properties to biomedical applications. *Gels, 8*(3), 167.

Ajji, Z., Jafari, A., Mousavi, A., Ajji, A., Heuzey, M.-C., & Savoji, H. (2025). 3D bioprinting of thick core–shell vascularized scaffolds for potential tissue engineering applications. *European Polymer Journal, 222*, Article 113564.

Annabi, N., Nichol, J. W., Zhong, X., Ji, C., Koshy, S., Khademhosseini, A., & Dehghani, F. (2010). Controlling the porosity and microarchitecture of hydrogels for tissue engineering. *Tissue Engineering Part B: Reviews, 16*(4), 371–383.

Ashraf, M. U., Hussain, M. A., Bashir, S., Haseeb, M. T., & Hussain, Z. (2018). Quince seed hydrogel (glucuronoxylan): Evaluation of stimuli responsive sustained release oral drug delivery system and biomedical properties. *Journal of Drug Delivery Science and Technology, 45*, 455–465.

Baniasadi, H., Polez, R. T., Kimiaei, E., Madani, Z., Rojas, O. J., Österberg, M., & Seppälä, J. (2021). 3D printing and properties of cellulose nanofibrils-reinforced quince seed mucilage bio-inks. *International Journal of Biological Macromolecules, 192*, 1098–1107.

Bencherif, S. A., Srinivasan, A., Horkay, F., Hollinger, J. O., Matyjaszewski, K., & Washburn, N. R. (2008). Influence of the degree of methacrylation on hyaluronic acid hydrogels properties. *Biomaterials, 29*(12), 1739–1749.

Bhatt, K., Eggermont, L. J., & Bencherif, S. A. (2022). Polymeric scaffolds for antitumor immune cell priming. In *Engineering technologies and clinical translation* (pp. 63–95). Elsevier.

Budday, S., Ovaert, T. C., Holzapfel, G. A., Steinmann, P., & Kuhl, E. (2020). Fifty shades of brain: A review on the mechanical testing and modeling of brain tissue. *Archives of Computational Methods in Engineering, 27*, 1187–1230.

Chen, J., Zhai, Z., & Edgar, K. J. (2022). Recent advances in polysaccharide-based in situ forming hydrogels. *Current Opinion in Chemical Biology, 70*, Article 102200.

Chen, Y., Liu, T., Wang, G., Liu, J., Zhao, L., & Yu, Y. (2020). Highly swelling, tough intelligent self-healing hydrogel with body temperature-response. *European Polymer Journal, 140*, Article 110047.

Christo, S. N., Diener, K. R., Bachhuka, A., Vasilev, K., & Hayball, J. D. (2015). Innate immunity and biomaterials at the nexus: Friends or foes. *BioMed Research International, 2015*.
Coleman, C. M., Auker, K. M., Killday, K. B., Azadi, P., Black, I., & Ferreira, D. (2019). Arabinoxyloglucan oligosaccharides may contribute to the antiadhesive properties of porcine urine after cranberry consumption. *Journal of Natural Products, 82*(3), 589–605.
Colombani, T., Eggermont, L. J., Hatfield, S. M., Rogers, Z. J., Rezaeeyazdi, M., Memic, A., … Bencherif, S. A. (2021). Oxygen-generating cryogels restore T cell mediated cytotoxicity in hypoxic tumors. *Advanced Functional Materials, 31*(37), Article 2102234.
Colombani, T., Eggermont, L. J., Rogers, Z. J., McKay, L. G., Avena, L. E., Johnson, R. I., … Bencherif, S. A. (2021). Biomaterials and oxygen join forces to shape the immune response and boost COVID-19 vaccines. *Advanced Science, 8*(18), Article 2100316.
Colombani, T., Rogers, Z. J., Bhatt, K., Sinoimeri, J., Gerbereux, L., Hamrangsekachaee, M., & Bencherif, S. A. (2023). Hypoxia-inducing cryogels uncover key cancer-immune cell interactions in an oxygen-deficient tumor microenvironment. *Bioactive Materials, 29*, 279–295.
Darvishi, E., Kahrizi, D., Arkan, E., Hosseinabadi, S., & Nematpour, N. (2021). Preparation of bio-nano bandage from quince seed mucilage/ZnO nanoparticles and its application for the treatment of burn. *Journal of Molecular Liquids, 339*, Article 116598.
Davenport Huyer, L., Bannerman, A. D., Wang, Y., Savoji, H., Knee-Walden, E. J., Brissenden, A., … Amsden, B. G. (2019). One-pot synthesis of unsaturated polyester bioelastomer with controllable material curing for microscale designs. *Advanced Healthcare Materials, 8*(16), Article 1900245.
De France, K. J., Xu, F., & Hoare, T. (2018). Structured macroporous hydrogels: Progress, challenges, and opportunities. *Advanced Healthcare Materials, 7*(1), Article 1700927.
Di Muzio, L., Paolicelli, P., Trilli, J., Petralito, S., Carriero, V. C., Brandelli, C., … Casadei, M. A. (2022). Insights into the reaction of chondroitin sulfate with glycidyl methacrylate: 1D and 2D NMR investigation. *Carbohydrate Polymers, 296*, Article 119916.
Ding, Y.-W., Zhang, X.-W., Mi, C.-H., Qi, X.-Y., Zhou, J., & Wei, D.-X. (2022). Recent advances in hyaluronic acid-based hydrogels for 3D bioprinting in tissue engineering applications. *Smart Materials in Medicine, 4*, 59–68.
Echalier, C., Valot, L., Martinez, J., Mehdi, A., & Subra, G. (2019). Chemical cross-linking methods for cell encapsulation in hydrogels. *Materials Today Communications, 20*, Article 100536.
Faramarzi, N., Yazdi, I. K., Nabavinia, M., Gemma, A., Fanelli, A., Caizzone, A., … Ruskin, J. N. (2018). Patient-specific bioinks for 3D bioprinting of tissue engineering scaffolds. *Advanced Healthcare Materials, 7*(11), Article 1701347.
Firipis, K., Footner, E., Boyd-Moss, M., Dekiwadia, C., Nisbet, D., Kapsa, R. M., … Quigley, A. (2022). Biodesigned bioinks for 3D printing via divalent crosslinking of self-assembled peptide-polysaccharide hybrids. *Materials Today Advances, 14*, Article 100243.
Ghumman, S. A., Mahmood, A., Noreen, S., Rana, M., Hameed, H., Ijaz, B., … ur Rehman, M. F.. (2022). Formulation and evaluation of quince seeds mucilage–sodium alginate microspheres for sustained delivery of cefixime and its toxicological studies. *Arabian Journal of Chemistry, 15*(6), Article 103811.
Guilherme, M. R., Reis, A. V., Takahashi, S. H., Rubira, A. F., Feitosa, J. P., & Muniz, E. C. (2005). Synthesis of a novel superabsorbent hydrogel by copolymerization of acrylamide and cashew gum modified with glycidyl methacrylate. *Carbohydrate Polymers, 61*(4), 464–471.
Guo, J. L., Li, A., Kim, Y. S., Xie, V. Y., Smith, B. T., Watson, E., … Mikos, A. G. (2020). Click functionalized, tissue-specific hydrogels for osteochondral tissue engineering. *Journal of Biomedical Materials Research Part A, 108*(3), 684–693.
Guzelgulgen, M., Ozkendir-Inanc, D., Yildiz, U. H., & Arslan-Yildiz, A. (2021). Glucuronoxylan-based quince seed hydrogel: A promising scaffold for tissue engineering applications. *International Journal of Biological Macromolecules, 180*, 729–738.
Handorf, A. M., Zhou, Y., Halanski, M. A., & Li, W.-J. (2015). Tissue stiffness dictates development, homeostasis, and disease progression. *Organogenesis, 11*(1), 1–15.
Huang, J., Fu, S., & Gan, L. (2019). *Lignin chemistry and applications*. Elsevier.
Hussain, M. A., Muhammad, G., Haseeb, M. T., & Tahir, M. N. (2019). Quince seed mucilage: A stimuli-responsive/smart biopolymer. *Funct Biopolym*, 1–22.
Jafari, A., Farahani, M., Sedighi, M., Rabiee, N., & Savoji, H. (2022). Carrageenans for tissue engineering and regenerative medicine applications: A review. *Carbohydrate Polymers, 281*, Article 119045.
Jafari, A., Hassanajili, S., Azarpira, N., Karimi, M. B., & Geramizadeh, B. (2019). Development of thermal-crosslinkable chitosan/maleic terminated polyethylene glycol hydrogels for full thickness wound healing: In vitro and in vivo evaluation. *European Polymer Journal, 118*, 113–127.
Jafari, A., Vahid Niknezhad, S., Kaviani, M., Saleh, W., Wong, N., Van Vliet, P. P., … Savoji, H. (2024). Formulation and evaluation of PVA/gelatin/carrageenan inks for 3D printing and development of tissue-engineered heart valves. *Advanced Functional Materials, 34*(7), Article 2305188.
Jin, M., Shi, J., Zhu, W., Yao, H., & Wang, D.-A. (2021). Polysaccharide-based biomaterials in tissue engineering: A review. *Tissue Engineering Part B: Reviews, 27*(6), 604–626.
Kim, J., Bencherif, S. A., Li, W. A., & Mooney, D. J. (2014). Cell-friendly inverse opal-like hydrogels for a spatially separated co-culture system. *Macromolecular Rapid Communications, 35*(18), 1578–1586.
Koyyada, A., & Orsu, P. (2021). Natural gum polysaccharides as efficient tissue engineering and drug delivery biopolymers. *Journal of Drug Delivery Science and Technology, 63*, Article 102431.
Laine, C., Tamminen, T., Vikkula, A., & Vuorinen, T. (2002). *Methylation analysis as a tool for structural analysis of wood polysaccharides*.
Lantigua, D., Nguyen, M. A., Wu, X., Suvarnapathaki, S., Kwon, S., Gavin, W., & Camci-Unal, G. (2020). Synthesis and characterization of photocrosslinkable albumin-based hydrogels for biomedical applications. *Soft Matter, 16*(40), 9242–9252.
Lee, A., Hudson, A., Shiwarski, D., Tashman, J., Hinton, T., Yerneni, S., Bliley, J., Campbell, P., & Feinberg, A. (2019). 3D bioprinting of collagen to rebuild components of the human heart. *Science, 365*(6452), 482–487.
Lim, K. S., Galarraga, J. H., Cui, X., Lindberg, G. C., Burdick, J. A., & Woodfield, T. B. (2020). Fundamentals and applications of photo-cross-linking in bioprinting. *Chemical Reviews, 120*(19), 10662–10694.
Lockett, C., Busza, A., Proctor, E., Churchill, T., Williams, S., & Fuller, B. (1996). Proton nuclear magnetic resonance spectroscopy of lactate production in isolated rat liver during cold preservation. *Cryobiology, 33*(2), 271–275.
Mahdavi, S., Amirsadeghi, A., Jafari, A., Niknezhad, S. V., & Bencherif, S. A. (2021). Avian egg: A multifaceted biomaterial for tissue engineering. *Industrial & Engineering Chemistry Research, 60*(48), 17348–17364.
Nicodemus, G. D., & Bryant, S. J. (2008). Cell encapsulation in biodegradable hydrogels for tissue engineering applications. *Tissue Engineering Part B: Reviews, 14*(2), 149–165.
Ouyang, L., Yao, R., Zhao, Y., & Sun, W. (2016). Effect of bioink properties on printability and cell viability for 3D bioplotting of embryonic stem cells. *Biofabrication, 8*(3), Article 035020.
Pereira, R. F., & Bártolo, P. J. (2015). 3D photo-fabrication for tissue engineering and drug delivery. *Engineering, 1*(1), 090–112.
Qi, J., Yan, Y., Cheng, B., Deng, L., Shao, Z., Sun, Z., & Li, X. (2018). Enzymatic formation of an injectable hydrogel from a glycopeptide as a biomimetic scaffold for vascularization. *ACS Applied Materials & Interfaces, 10*(7), 6180–6189.
Reis, A. V., Fajardo, A. R., Schuquel, I. T., Guilherme, M. R., Vidotti, G. J., Rubira, A. F., & Muniz, E. C. (2009). Reaction of glycidyl methacrylate at the hydroxyl and carboxylic groups of poly (vinyl alcohol) and poly (acrylic acid): Is this reaction mechanism still unclear? *The Journal of Organic Chemistry, 74*(10), 3750–3757.
Rezaeeyazdi, M., Colombani, T., Eggermont, L. J., & Bencherif, S. A. (2022). Engineering hyaluronic acid-based cryogels for CD44-mediated breast tumor reconstruction. *Materials Today Bio, 13*, Article 100207.
Savoji, H., Davenport Huyer, L., Mohammadi, M. H., Lun Lai, B. F., Rafatian, N., Bannerman, D., … Radisic, M. (2020). 3D printing of vascular tubes using bioelastomer prepolymers by freeform reversible embedding. *ACS Biomaterials Science & Engineering, 6*(3), 1333–1343.
Schwab, A., Levato, R., D'Este, M., Piluso, S., Eglin, D., & Malda, J. (2020). Printability and shape fidelity of bioinks in 3D bioprinting. *Chemical Reviews, 120*(19), 11028–11055.
Şimşek, E., Karaca, B., & Arslan, Y. E. (2020). Bioengineered three-dimensional physical constructs from quince seed mucilage for human adipose-derived mesenchymal stem cells. *Journal of Bioactive and Compatible Polymers, 35*(3), 240–253.
Su, T., Xu, M., Lu, F., & Chang, Q. (2022). Adipogenesis or osteogenesis: Destiny decision made by mechanical properties of biomaterials. *RSC Advances, 12*(38), 24501–24510.
Tiwari, S., Patil, R., & Bahadur, P. (2018). Polysaccharide based scaffolds for soft tissue engineering applications. *Polymers, 11*(1), 1.
Tsanaktsidou, E., Kammona, O., & Kiparissides, C. (2022). Recent developments in hyaluronic acid-based hydrogels for cartilage tissue engineering applications. *Polymers, 14*(4), 839.
Unagolla, J. M., & Jayasuriya, A. C. (2020). Hydrogel-based 3D bioprinting: A comprehensive review on cell-laden hydrogels, bioink formulations, and future perspectives. *Applied Materials Today, 18*, Article 100479.
Velasco-Rodriguez, B., Diaz-Vidal, T., Rosales-Rivera, L. C., García-González, C. A., Alvarez-Lorenzo, C., Al-Modlej, A., … Soltero Martínez, J. F. A. (2021). Hybrid methacrylated gelatin and hyaluronic acid hydrogel scaffolds. Preparation and systematic characterization for prospective tissue engineering applications. *International Journal of Molecular Sciences, 22*(13), 6758.
Wang, L., Liu, H.-M., & Qin, G.-Y. (2017). Structure characterization and antioxidant activity of polysaccharides from Chinese quince seed meal. *Food Chemistry, 234*, 314–322.
Wang, S., Chen, Y., Ling, Z., Li, J., Hu, J., He, F., & Chen, Q. (2022). The role of dendritic cells in the immunomodulation to implanted biomaterials. *International Journal of Oral Science, 14*(1), 52.
Yilmaz, H. D., Cengiz, U., Arslan, Y. E., Kiran, F., & Ceylan, A. (2021). From a plant secretion to the promising bone grafts: Cryogels of silicon-integrated quince seed mucilage by microwave-assisted sol–gel reaction. *Journal of Bioscience and Bioengineering, 131*(4), 420–433.
Yilmaz, H. D., Cengiz, U., Derkus, B., & Arslan, Y. E. (2023). Development of plant-based biopolymer coatings for 3D cell culture: Boron–silica-enriched quince seed mucilage nanocomposites. *Biomaterials Science, 11*(15), 5320–5336.
Yoon, J. A., Bencherif, S. A., Aksak, B., Kim, E. K., Kowalewski, T., Oh, J. K., & Matyjaszewski, K. (2011). Thermoresponsive hydrogel scaffolds with tailored hydrophilic pores. *Chemistry, an Asian Journal, 6*(1), 128–136.
Yu, C., Schimelman, J., Wang, P., Miller, K. L., Ma, X., You, S., … Chen, S. (2020). Photopolymerizable biomaterials and light-based 3D printing strategies for biomedical applications. *Chemical Reviews, 120*(19), 10695–10743.
Zhao, Y., Kang, J., & Tan, T. (2006). Salt-, pH-and temperature-responsive semi-interpenetrating polymer network hydrogel based on poly (aspartic acid) and poly (acrylic acid). *Polymer, 47*(22), 7702–7710.

Further Reading

Xie, A.-J., Yin, H.-S., Liu, H.-M., Zhu, C.-Y., & Yang, Y.-J. (2018). Chinese quince seed gum and poly (N, N-diethylacryl amide-co-methacrylic acid) based pH-sensitive hydrogel for use in drug delivery. *Carbohydrate Polymers, 185*, 96–104.